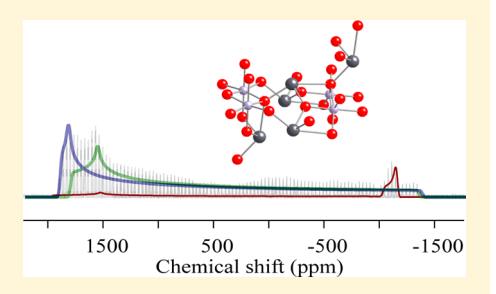
²⁰⁷Pb and ¹¹⁹Sn Solid-State NMR and Relativistic Density Functional Theory Studies of the Historic Pigment Lead-Tin Yellow Type I and Its Reactivity in Oil Paintings

Jaclyn Catalano, †,‡ Anna Murphy,‡ Yao Yao,‡ Fahri Alkan,‡ Nicholas Zumbulyadis,§ Silvia A. Centeno,† and Cecil Dybowski*,‡

Supporting Information

ABSTRACT: Lead soaps (lead carboxylates) have been detected in traditional oil paintings in layers containing the pigment lead-tin yellow type I (LTY-I). LTY-I has been used by artists from at least the second quarter of the 15th century until the first half of the 18th century. Soap formation can lead to protrusions in paint layers and increased transparency, causing the paint support to become visible. We have characterized LTY-I by 119 Sn and 207 Pb solid-state NMR (ssNMR) spectroscopy. Using a combination of NMR techniques and DFT molecular cluster calculations, we identify the individual species in LTY-I and determine their ¹¹⁹Sn and ²⁰⁷Pb chemical-shift tensors. The presence of starting materials from the synthesis, minium, and tin(IV) oxide was also verified. Knowledge of the chemical-



shift tensor components and the impurities in LTY-I is important for examining the chemistry of degradation processes and soap formation. We demonstrate that ssNMR can be used to detect reaction between Pb2SnO4 and added palmitic acid in a model paint sample containing LTY-I.

■ INTRODUCTION

Lead-tin yellow type I (LTY-I) was used as a pigment in European paintings from at least the second quarter of the 15th century until the first half of the 18th century. 1,2 This pigment is an important source of lead ions and has been implicated in the formation of lead carboxylates (commonly referred to as lead soaps), second only to basic lead white, 2PbCO₃. Pb(OH)₂.³ Lead soap formation is a process that has been observed in hundreds of oil paintings and manifests itself in the formation of aggregates 100-200 µm in diameter that distort the paintings' surface textures, by an increased transparency of the paint films, or by the formation of surface crusts.³⁻⁹ In recent years characterizing the reactivity of lead stannate, Pb₂SnO₄, with fatty acids has been increasingly recognized as a key issue to understand soap formation in paintings.^{3,10}

LTY-I can be prepared by heating a mixture of massicot (orthorhombic PbO) or minium (Pb3O4) with tin(IV) oxide (SnO₂) and, depending on the manufacturing conditions, this process may lead to mixtures of the orthorhombic form Pb₂SnO₄ with the cubic PbSnO₃ and PbO. It has been stated that when following historic recipes, the optimum temperature range for the synthesis of pure Pb2SnO4 is between 800 and 900 °C. 11 Commercial sources report the empirical formula of the pigment as $PbSn_xO_y$. It is not clear whether this ambiguous stoichiometry implies the presence of distinct phases or a solid solution. A similar ambiguity exists concerning the pigment as used in works of art. Single crystals of Pb₂SnO₄ have been grown, 12 and powder X-ray diffraction and Raman data have been published 11,13-15 showing scant information on the existence and nature of more complex phases. Yet, it is these minor components that are assumed to react with the free fatty acids in the binding medium of oil paintings.³ Therefore, solidstate nuclear magnetic resonance (ssNMR) characterization of LTY-I is important for determining the chemical species present in LTY-I, and which species are responsible for soap formation. We use model paint samples to study the reactivity of LTY-I, because only microscopic heterogeneous samples can be obtained from paintings.

Recently, we have demonstrated that ssNMR is a useful technique for obtaining local structural information on lead soaps that cannot be accessed by other methods. 16 A combination of NMR pulse sequences was used because lead has a large chemical-shift anisotropy and correspondingly broad powder patterns. The Wideband Uniform Rate Smooth Truncation-Carr-Purcell-Meiboom-Gill (WURST-CPMG) pulse sequence has been proven simple to implement and advantageous in the acquisition of the ultrawideline ssNMR spectra of both spin 1/2 and quadrupolar nuclei. 17-21

In this contribution we use WURST-CPMG and magic angle spinning (MAS) experiments to measure the ¹¹⁹Sn and ²⁰⁷Pb

Received: June 13, 2014 Revised: August 21, 2014 Published: August 21, 2014

[†]Department of Scientific Research, The Metropolitan Museum of Art, New York, New York 10028, United States

[‡]Department of Chemistry and Biochemistry, University of Delaware, Newark, Delaware 19716, United States

[§]Independent Researcher, Rochester, New York 14613, United States

chemical-shift tensors in LTY-I. The experimental results are supported by computational methods for the prediction of ²⁰⁷Pb NMR parameters from known structural parameters. We use a combination of efficient computational simulations and iterative fittings of the experimental and calculated data to extract the tensor components and assign the overlapping powder patterns to the two crystallographically inequivalent lead positions in the lattice. For such systems, calculations of NMR parameters involve two important considerations. First, relativistic effects must be included in the quantum chemical methods for heavy nuclei such as lead. ^{22–24} Second, appropriate modeling of the solid-state structure of the system is necessary to obtain meaningful NMR parameters. ^{25–27} The results of these calculations allow us to specify which experimental parameters apply to each of the two sites.

EXPERIMENTAL SECTION

Sample Preparation and SEM-EDS Analysis. LTY-I 1010 Light was purchased from Kremer Pigments (Germany). For the paint film, 2 g of LTY-I were mixed with 1 g of linseed oil and 0.5 g of palmitic acid. The wet paint film formed a thick paste that was spread on three slides and aged under laboratory conditions for 8 months (approximately 20 °C and 55% relative humidity). The sample was packed in a rotor for 3 weeks, before running the final spectra, showing full consumption of the palmitic acid to within 5%. The reaction was monitored using ¹³C NMR by integrating the carboxyl peaks of palmitic acid and lead palmitate.

Powder X-ray diffraction was used to confirm the geometry of our sample of LTY-I. 12,28 X-ray diffraction measurements were carried out in a Philips PW1835 open-architecture diffractometer using Cu K α (λ = 1.542 Å) radiation at an acceleration voltage of 45 kV and a 35-mA current. Elemental analysis was performed by energy dispersive X-ray spectrometry in the scanning electron microscope (SEM-EDS), using a FE-SEM Zeiss Σ igma HD spectrometer equipped with an Oxford Instrument X-Max N 80 SDD detector, with the SEM operated at an accelerating voltage of 20 kV. The atom percentages of lead and tin are normalized to 100%. These values, along with the signal percentages from NMR spectra, were used to calculate the mole percentage of each species in the LTY-I sample.

Experimental NMR Methods. ²⁰⁷Pb, ¹¹⁹Sn, and ¹³C ssNMR spectra were recorded at 11.75 T (104.63 MHz ²⁰⁷Pb frequency, 186.50 MHz ¹¹⁹Sn frequency, and 125.76 MHz ¹³C frequency) with a standard Bruker 4 mm probe. Approximately 100 mg of sample was packed in a 4 mm rotor. Solid lead nitrate was used as a secondary external reference for the ²⁰⁷Pb spectra, the isotropic chemical-shift being -3491 ppm relative to tetramethyllead (TML) at 298 K.²⁹ A plot of spinning speed versus the isotropic chemical shift of lead nitrate was obtained to compensate for the temperature increase due to spinning. SnCl₂ in HCl was used as a secondary external reference for the ¹¹⁹Sn spectra, the isotropic chemical shift being -388.1 ppm relative to tetramethyltin.³⁰ Glycine was used as a secondary external reference for the 13C spectra, with an isotropic chemical shift of the carboxyl peak of 176 ppm relative to tetramethylsilane.

²⁰⁷Pb spectra were acquired using direct excitation and highpower decoupling, with spin-temperature alternation and magic-angle spinning (STA/MAS) at 11 and 12 kHz to obtain isotropic chemical shifts. Spin-temperature alternation minimized the effects of acoustic ringing of the probe circuits. Acquisition parameters for these experiments included a π pulse width of 8.5 μ s, a delay of 1 ms, and a $\pi/2$ pulse width of 4.25 μ s. High-power proton decoupling (SPINAL-64 at 100 kHz) was used to suppress dipolar couplings. The recycle delay was 5 s and 40,000 scans were acquired.

 ^{207}Pb WURST-CPMG spectra of the samples were recorded using the parameters of MacGregor et al. 17 WURST pulse widths were 50 μ s, with pulse shapes created via the shape tool in Topspin 3.1. Seventy-five Meiboom—Gill loops were acquired for the WURST-CPMG experiments, with a 200 μ s echo, and a sweep range of 0.5 MHz in all cases. The recycle delay was 7 s. High-power proton decoupling (CW at 100 kHz) was used to suppress dipolar couplings. Multiple WURST-CPMG spectra were collected at different carrier frequencies by shifting the carrier frequency a multiple of the spikelet separation (981.934 ppm) from spectrum to spectrum. Each spectrum was 10 240 scans. The collected spectra were superimposed to form the final spectrum.

¹¹⁹Sn spectra were acquired using direct excitation with STA/MAS at 5 and 12 kHz with 1024 and 564 scans, respectively. Acquisition parameters for these experiments included a π pulse width of 5.2 μ s, a delay of 1 ms, and a π /2 pulse width of 2.6 μ s. High-power proton decoupling (SPINAL-64 at 100 kHz) was used to suppress dipolar couplings. The recycle delay was 5 s.

¹³C spectra were acquired using cross-polarization with MAS at 12 kHz. Acquisition parameters for these experiments included a contact time of 1 ms and a recycle delay of 5 s. During acquisition, proton decoupling (SPINAL-64 at 100 kHz) was used to suppress dipolar couplings.

The analysis of the ²⁰⁷Pb chemical-shift tensors was performed by fitting the WURST-CPMG envelope using the previously published tensor for minium.³¹ The values of the isotropic chemical shifts were determined from STA/MAS spectra, with the help of DFT calculations. Fits to the WURST-CPMG envelopes were aided by simulation of the powder pattern with the program WSOLIDS.³² The ¹¹⁹Sn chemical-shift tensors were determined using the isotropic chemical shifts determined by spinning at 12 kHz and fitting the spinning sideband pattern from the spectrum at 5 kHz using HBA 3.1.³² From the fits, we were able to determine the relative mole percentage of each species.

Computational Methods. The chemical-shielding tensor can be represented as a 3×3 matrix in a Cartesian coordinate system. In the principal axis system (PAS), the shielding tensor is diagonal and the principal components are conventionally assigned as $\sigma_{11} \leq \sigma_{22} \leq \sigma_{33}$, which is known as the frequency-ordered convention. NMR experiments measure the chemical-shift related to the principal components of the chemical-shielding tensor by eq 1.

$$\delta_{ii} = \frac{\sigma_{\text{ref}} - \sigma_{ii}}{1 - \sigma_{\text{ref}}} \tag{1}$$

For heavy nuclei such as ^{207}Pb , the calculated σ_{ref} is usually of the order of $10^{-3}-10^{-4}$. For this reason, the calculated shieldings are converted to chemical shifts by explicit inclusion of the factor $(1 - \sigma_{\text{ref}})$.

It is possible to define the chemical-shift tensor using alternative sets of parameters. A convenient description for the NMR spectra of powders is given by the Maryland convention.³⁴ In this convention the powder pattern is defined by the isotropic chemical shift (δ_{iso}), the span (Ω), and the

skew (κ). These three parameters are related to the principal components by the following relations:

$$\delta_{\rm iso} = \frac{1}{3} (\delta_{11} + \delta_{22} + \delta_{33}) \tag{2}$$

$$\Omega = |\delta_{11} - \delta_{33}| \tag{3}$$

$$\kappa = \frac{3(\delta_{22} - \delta_{\rm iso})}{\Omega} \tag{4}$$

All density functional computations were performed using the Amsterdam Density Functional (ADF v2013) program package. The calculations were carried out at the DFT/BP86 level. For the calculations we employed a molecular-cluster approach in which the clusters are formed from the experimental X-ray geometry. The molecular clusters are shown in Figure 1. For clusters I and II, the TZ2P/all-electron (AE) basis set was used for all atoms in the cluster.

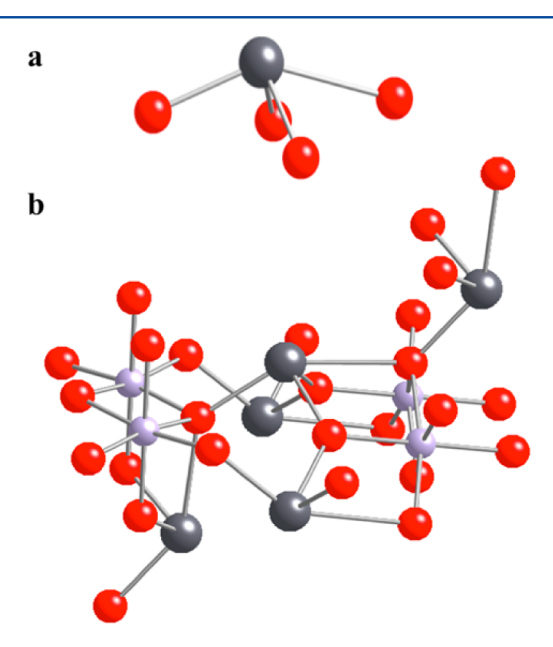


Figure 1. Molecular clusters of lead—tin yellow employed in the computational investigations, lead (dark gray), oxygen (red), and tin (light gray). Cluster I (a) and cluster II (b).

For all calculations, relativistic effects were included in the ZORA Hamiltonian at the spin—orbit level. $^{40-43}$ The NMR parameters were computed within the GIAO formalism. $^{44-46}$ To deal with dangling bonds and resulting self-consistent-field (SCF) convergence problems, the terminal oxygen atoms were saturated with hydrogens. The reported chemical shifts are referenced to the extrapolated intercept of the best-fit correlation line for calculations of the principal components of the chemical shielding of clusters of α - and β -PbO (7933 ppm); see Supporting Information Figure S1.

DISCUSSION OF RESULTS

Determination of the ²⁰⁷Pb Chemical-Shift Tensors. Crystallographically, Pb₂SnO₄ belongs to the *Pbam* space group, with two distinct lead sites¹¹ (labeled as Pb(1) and Pb(2)) that theoretically give rise to two distinct NMR signals. However, there are only minimal differences in the local geometries of the lead sites. Both lead sites are coordinated to four oxygen atoms in a hemidirected fashion (Figure 2), similar

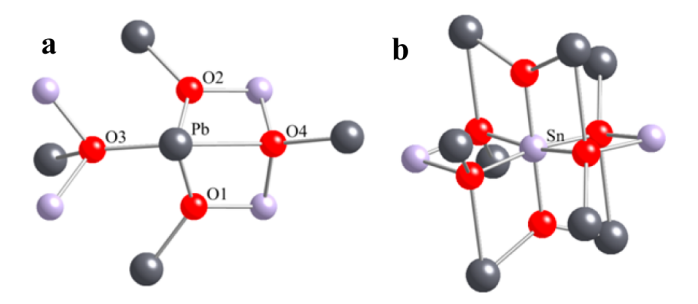


Figure 2. Structure of Pb_2SnO_4 showing the coordination environment around the (a) lead (dark gray) and (b) tin (light gray) sites. Oxygen is shown in red. Pb(1) and Pb(2) are structurally similar, and both would have similar environments with slight differences in bond lengths and bond angles.

to other lead oxides like α -PbO and β -PbO. ^{47,48} As reported in Table 1, for Pb(1), two oxygen atoms are bonded to lead with

Table 1. Selective Bond Distances (Å) and Angles (deg) for the First Coordination Shells of Pb(1) and Pb(2) in Pb_2SnO_4

	Pb(1)	Pb(2)
Pb-O1	2.15	2.24
Pb-O2	2.15	2.24
Pb-O3	2.33	2.29
Pb-O4	2.78	2.80
O1-Pb-O2	94.14	89.22
O1-Pb-O3	90.64	88.64
O2-Pb-O3	90.64	88.64

the same bond distance (2.15 Å) and an O-Pb-O angle of 94.14°. The other Pb-O distances are 2.33 and 2.78 Å. For Pb(2), the two equivalent Pb-O bond distances are 2.24 Å and the O-Pb-O angle is 89.22°. The other two Pb-O bond lengths are 2.80 and 2.29 Å.

The 207 Pb spectra of LTY-I were obtained using the STA/MAS and WURST-CPMG experiments. The STA/MAS spectrum with the carrier frequency set at 1650 ppm (Figure S2, Supporting Information) pointed to a broad powder pattern that was not uniformly excited and the spinning sideband pattern for the two lead sites could not be resolved. This was true for MAS spinning speeds of 11 and 12 kHz. However, when the carrier was moved to -1000 ppm, peaks for an impurity were clearly visible. The minium Pb(IV) site was identified with an isotropic chemical-shift of -1102 ± 4 ppm (Figure S3, Supporting Information). 31,49 Minium is a starting material for the synthesis of LTY-I as well as a photo-degradation product of the pigment. 14

To achieve uniform excitation and determine the principal components of the ^{207}Pb chemical-shift tensors accurately, we recorded WURST-CPMG spectra piecewise by shifting the carrier frequency an integer multiple of the spikelet spacing. Figure 3 shows the fit of the total spectrum, which consists of the overlap of the chemical-shift tensors of four lead species, two having similar chemical-shift tensors assigned to Pb_2SnO_4 and the Pb(II) and Pb(IV) sites of the minium impurity that have been previously reported. 31 The two tensors arising from the dominant Pb_2SnO_4 in LTY-I were refined by determining the possible isotropic chemical shifts from STA/MAS experiments and DFT calculations of the skew. The experimentally determined chemical-shift tensors are reported in Table 2. The

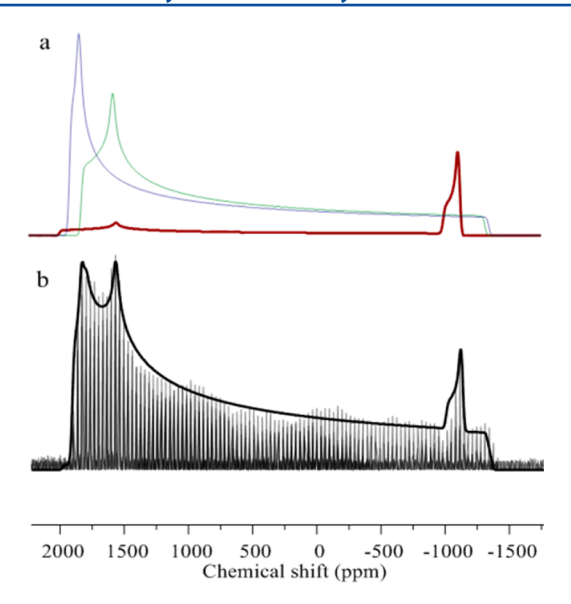


Figure 3. (a) Simulated spectrum for each of the individual components in the sample. Pb₂SnO₄ (blue and green) and the impurity minium (red). (b) ²⁰⁷Pb spectrum of LTY-I obtained with WURST-CPMG, showing four lead species.

integrated intensities for the species in the simulated fit of the WURST-CPMG spectrum gave 92.5 \pm 1.5% of the lead as Pb₂SnO₄ and 7.5 \pm 1.5% as minium.

Calculation of ²⁰⁷Pb Chemical-Shielding Tensors. In Table 2, calculated NMR parameters for different clusters that represent Pb₂SnO₄ (Figure 1) at the AE level of theory are tabulated. Calculations on the cluster that includes only the first co-ordination shell (cluster I) fail to reproduce the experimentally determined chemical-shift principal components, as expected. The first coordination shell cluster is not large enough to describe the interactions necessary for an accurate calculation of the NMR parameters. Cluster II describes the effects of higher coordination shells, for which the calculated parameters are improved significantly over the parameters of cluster I.

Another important aspect of this investigation is the assignment of experimental NMR parameters to a lead site by using general symmetry arguments that correlate the ssNMR and computational results. From the experimentally resolved parameters, the most obvious difference is the resonance position of δ_{22} relative to δ_{11} . For the experimental tensor of lead site B, δ_{11} and δ_{22} are very close to each other. The difference between the two experimental principal components is only 75 ppm. For the experimental tensor of lead site A, this difference is 250 ppm, mostly due to a shift of δ_{22} . From a

comparison of the calculated parameters of Pb_2SnO_4 for both clusters, the difference between δ_{11} and δ_{22} is larger for the Pb(1) site than for Pb(2). The difference is particularly obvious for cluster II where $|\delta_{11} - \delta_{22}|$ is 182 ppm for Pb(1) and 68 ppm for Pb(2). Thus, we make the assignment of Pb(1) and Pb(2) to experimental sites A and B, respectively.

As mentioned earlier, the local X-ray-derived structures of the two lead sites are similar. The structure around Pb(1) is illustrated in Figure 2a. Because the differences in the two coordination environments are due to differences in the bond lengths and angles, a similar picture can be drawn for Pb(2). The bond distances and angles around the lead centers in the first co-ordination shell are tabulated in Table 1. From the local structure of Pb(2), it is seen that O1, O2, and O3 have a quasi- $C_{3\nu}$ symmetry around the lead center. This symmetry is perturbed by the presence of O4 and the perturbation is larger for Pb(1) than for Pb(2). Therefore, one would expect the NMR parameters of Pb(2) to deviate slightly from the condition $\delta_{11} = \delta_{22} > \delta_{33}$ expected for perfect $C_{3\nu}$ symmetry. Furthermore, the deviation would be expected to be larger for Pb(1). This expectation is confirmed by the calculations, as seen for the sufficiently large cluster II.

Determination of the ¹¹⁹Sn Chemical-Shift Tensors. The ¹¹⁹Sn spectrum of LTY-I was recorded with the STA/MAS sequence at 12 and 5 kHz (Figure 4). Two tin species are

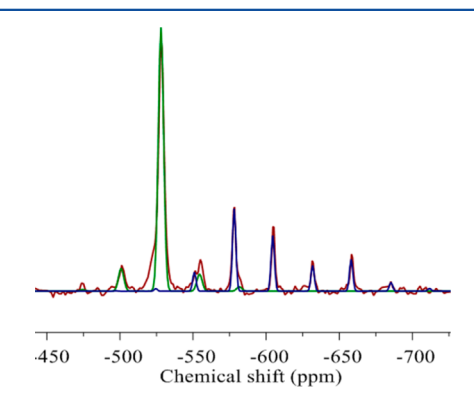


Figure 4. Experimental ¹¹⁹Sn STA/MAS with proton decoupling spectrum (red) of the LTY-I sample recorded on a 500 MHz magnet, showing unreacted starting material SnO_2 . The percentages of the two tin species were determined using MAS simulations in WSOLIDS with $64 \pm 2\%$ for Pb_2SnO_4 (green) and $36 \pm 2\%$ for SnO_2 (blue).

present; one is the tin site of Pb_2SnO_4 , and the other is the tin site of SnO_2 , one of the starting materials for the synthesis of LTY-I. As seen in Figure 2, the coordination geometry around the tin site in Pb_2SnO_4 is close to spherical symmetry. This is

Table 2. Calculated and Experimental Principal Components of the ²⁰⁷Pb Chemical-Shift Tensors of Pb₂SnO₄^a

model clusters	$\delta_{11}~(\mathrm{ppm})$	$\delta_{22}~(\mathrm{ppm})$	$\delta_{33}~(\mathrm{ppm})$	$\delta_{ m iso}$ (ppm)	Ω (ppm)	κ
experiment site A	1810 ± 7	1565 ± 10	-1335 ± 20	690 ± 23	3145 ± 21	0.84 ± 0.02
experiment site B	1903 ± 7	1828 ± 7	-1365 ± 25	789 ± 27	3268 ± 26	0.95 ± 0.03
cluster I						
Pb(1)	-416	-871	-2181	-1156	1765	0.48
Pb(2)	-617	-946	-2023	-1195	1445	0.53
cluster II						
Pb(1)	1987	1805	-1145	882	3132	0.88
Pb(2)	1802	1734	-1206	777	3008	0.95

^aSpan (Ω) and skew (κ) were calculated. $\Omega = |\delta_{33} - \delta_{11}|$ and $\kappa = 3*(\delta_{iso} - \delta_{22})/\Omega$.

Table 3. Principal Components of the 119Sn Chemical-Shift Tensors of Species Found in Lead-Tin Yellow I

material	$\delta_{11}~(\mathrm{ppm})$	$\delta_{22}~(\mathrm{ppm})$	$\delta_{33}~(\mathrm{ppm})$	$\delta_{ m iso}$ (ppm)	Ω (ppm)	κ
SnO_2	-558 ± 3	-566 ± 4	-692 ± 5	-605 ± 4	134 ± 6	0.87 ± 0.09
Pb_2SnO_4	-515 ± 4	-517 ± 5	-556 ± 7	-529 ± 5	41 ± 6	0.88 ± 0.14

reflected in the principal components of the chemical-shift tensor derived from a fit of the spectrum in Figure 4, showing a small span indicative of a nearly spherically symmetric environment. The principal components of the Pb_2SnO_4 chemical-shift tensors are given in Table 3. They were determined by fitting the spinning sideband pattern at 5 kHz with the STA/MAS experiment and the isotropic chemical shifts obtained at 12 kHz. The tensor determined for SnO_2 is in agreement with various literature reports that the isotropic chemical shift is -604 ± 1 ppm with spans from 121 to 136 ppm. $^{51-54}$

The integrated intensities of the two species in the simulation of the 119 Sn STA/MAS spectrum (Figure 4) are $64 \pm 2\%$ tin as Pb_2SnO_4 and $36 \pm 2\%$ as SnO_2 . Using the fits of the 207 Pb WURST-CPMG and 119 Sn STA/MAS spectra, along with the elemental atom percentages determined by SEM-EDS, we calculated the mole percentages of the molecular species in the sample, as shown in Table 4. With these results, we find that for

Table 4. Normalized Mole Percentages of Lead and Tin Determined from SEM-EDS and NMR

	method	lead	tin
LTY-I	SEM-EDS	56.3 ± 0.3	43.7 ± 0.4
Pb_2SnO_4	NMR Calculated ^a	52.1 ± 0.9	28.0 ± 0.9
Pb_3O_4		4.2 ± 0.8	
SnO_2			15.7 ± 0.9

^aCalculated from the signal % in the NMR spectrum and the SEM-EDS results.

every mole of Pb_2SnO_4 , there is 0.054 ± 0.011 mol of Pb_3O_4 present in this LTY-I sample. We also find that for every mole of Pb_2SnO_4 , there is 0.56 ± 0.04 mol of SnO_2 . From NMR, we detect no other species.

Reaction of LTY-I with Palmitic Acid. Because the soap formation process occurs over many years in cultural heritage objects, we have induced soap formation by adding free fatty acid when preparing paint films to investigate the chemistry of LTY-I. FT-IR (not shown), ¹³C NMR, and ²⁰⁷Pb NMR show the formation of lead palmitate (Figure 5), in agreement with previous measurements. The carboxyl region of Figure 5a indicates almost complete conversion of palmitic acid (180.4 ppm) to lead palmitate (182.6 and 183.8 ppm). ^{10,55} The ²⁰⁷Pb spectrum (Figure 5b) shows that minium is still observable, although the amount of palmitate formed (0.97 mmol of lead) should have exhausted the minium (0.45 mmol of lead) if it were the only source of lead. In Table 5 we report the ²⁰⁷Pb NMR signal percentages of Pb₂SnO₄ and Pb₃O₄ before and after reaction.

Compared to the ²⁰⁷Pb spectrum of LTY-I, the ¹¹⁹Sn spectrum is simpler and the tin species have chemical-shift tensors with smaller spans, making it easier to obtain spectra. Comparison of the relative intensities in the ¹¹⁹Sn spectrum of unreacted LTY-I with relative intensities in the ¹¹⁹Sn spectrum of the sample after reaction with palmitic acid shows that Pb₂SnO₄ is a source of lead to produce lead palmitate, Figure 6 and Table 5.

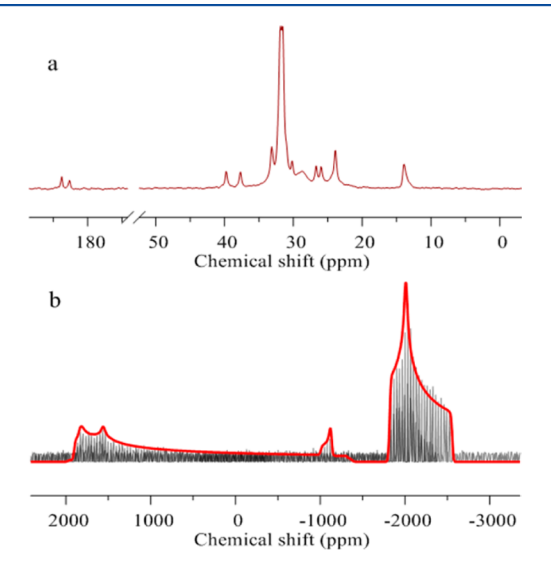


Figure 5. NMR spectra of the LTY-I paint film containing free palmitic acid. (a) 13 C MAS NMR spectrum, showing lead palmitate formation by the appearance of peaks at 182.6 and 183.8 ppm. (b) 207 Pb WURST-CPMG spectrum, showing in addition to Pb₂SnO₄, lead palmitate ($\delta_{iso} = -2131$ ppm), and minium ($\delta_{iso} = -1102$ ppm).

Table 5. NMR Signal Percentages before and after Reaction

	before reaction		after reaction		
	²⁰⁷ Pb	¹¹⁹ Sn	²⁰⁷ Pb	¹¹⁹ Sn	
Pb ₂ SnO ₄	92.5 ± 1.5	64 ± 2	86 ± 2	55 ± 2	
Pb_3O_4	7.5 ± 1.5		14 ± 2		
SnO_2		36 ± 2		45 ± 2	

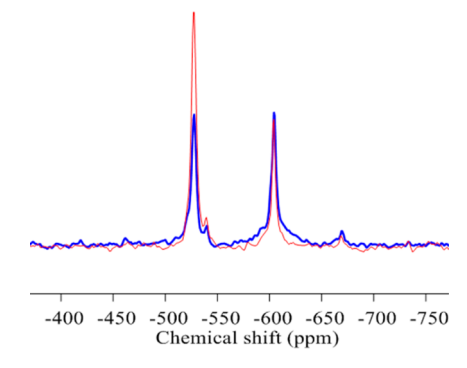


Figure 6. ¹¹⁹Sn STA/MAS NMR spectra of LTY-I before (red) and after reaction (blue) with palmitic acid in a paint film. The difference in the relative intensity of signal at -529 ppm from Pb_2SnO_4 in the two spectra demonstrates that Pb_2SnO_4 has been partially consumed as a result of reaction.

CONCLUSIONS

The materials encountered in cultural heritage objects are complex and heterogeneous. They are seldom chemically inert and their reactions follow complex pathways. Characterization of their structure and reactivity represents a formidable analytical challenge. We have demonstrated that high-quality

relativistic DFT calculations enable the assignment of the solidstate NMR spectra of crystallographically inequivalent heavy metal nuclides for Pb₂SnO₄. The calculated chemical-shift principal components for ²⁰⁷Pb deviate at most by 15% from the experimental ones. The combination of ssNMR and DFT molecular-cluster calculations is applicable to studies of other lead-containing materials, as well as solids containing other heavy nuclides.

In LTY-I, by ssNMR we have only detected minium and Pb₂SnO₄ as possible sources of lead ions for the formation of lead soaps. We have not detected the existence of other lead oxides in the unreacted pigment that have been proposed to be the source of lead reacting with the free fatty acids.³ Quantitative evaluation of NMR spectra of the unreacted paint with the material after reaction shows that Pb₂SnO₄ is a source of lead in the formation of lead soaps from lead—tin yellow. Whether the Pb₂SnO₄ participates directly in reaction with palmitic acid or it produces intermediates that react with the palmitic acid cannot be determined by these experiments. With the advancement of microrotors, these experiments could, in principle, be used to study samples from cultural heritage objects.

ASSOCIATED CONTENT

S Supporting Information

The best-fit correlation line for calculations of the principal components of the chemical shielding of clusters of α - and β -PbO and ²⁰⁷Pb STA/MAS spectra of LTY-I. This material is available free of charge via the Internet at http://pubs.acs.org.

AUTHOR INFORMATION

Corresponding Author

*C. Dybowski. E-mail: dybowski@udel.edu.

Notes

The authors declare no competing financial interest.

ACKNOWLEDGMENTS

C.D. acknowledges the support of the National Science Foundation under Grants CHEM-0956006 and CHE-1139192. S.C. acknowledges the support of the National Science Foundation under Grant CHEM-1139190. We acknowledge helpful discussions with Dr. Shi Bai and Dr. Guangjin Hou about the development of wide-band inversion and the spectroscopy of ²⁰⁷Pb. We thank Mark Wypyski from The Metropolitan Museum of Art for the SEM-EDS characterization of LTY-I.

REFERENCES

- (1) Eastaugh, N.; Walsh, V.; Chaplin, T.; Siddall, R. Pigment Compendium. A Dictionary of Historical Pigments; Elsevier Butterworth-Heinemann: Amsterdam, 2004.
- (2) Martin, E.; Duval, A. R. Les Deux Varietes de Jaune de Plomb et d'étain: Etude Chronologique. *Stud. Conserv.* **1990**, *35*, 117–136.
- (3) Keune, K. Binding Medium, Pigments and Metal Soaps Characterised and Localised in Paint Cross-Sections. Ph.D. Thesis, University of Amsterdam, Amsterdam, 2005.
- (4) Van der Weerd, J. Microspectroscopic Analysis of Traditional Oil Paint. Ph.D. Thesis, University of Amsterdam, Amsterdam, 2002.
- (5) Noble, P.; Boon, J. J.; Wadum, J. Dissolution, Aggregation and Protrusion. Lead Soap Formation in 17th Century Grounds and Paint Layers. *ArtMatters* **2003**, *1*, 46–61.
- (6) Higgitt, C.; Spring, M.; Saunders, D. Pigment-medium Interactions in Oil Paint Films Containing Red Lead or Lead Tin Yellow. *National Gallery Techn. Bull.* **2003**, 24, 75–91.

- (7) Cotte, M.; Checroun, E.; Susini, J.; Walter, P. Micro-analytical Study of Interactions Between Oil and Lead Compounds in Paintings. *Appl. Phys. A: Mater. Sci. Process.* **2007**, *89*, 841–848.
- (8) van Loon, A. Color Changes and Chemical Reactivity in Seventeenth-Century Oil Paintings. Ph.D. Thesis, University of Amsterdam, Amsterdam, 2008.
- (9) Mahon, D.; Centeno, S. A. A Technical Study of John Singer Sargent's Portrait of Madame Pierre Gautreau. *Metropol. Museum J.* **2005**, *40*, 121–129.
- (10) Boon, J. J.; Gore, E.; Keune, K.; Burnstock, A. Image Analytical Studies of Lead Soap Aggregates and thier Relationship to Lead and Tin in 15th Century Lead Tin Yellow Paints from the S Herbourne Triptych. In *Infrared and Raman User Group (IRUG) Meeting*; Picollo, M., Ed.; Florence, Italy, **2004**; pp 66–74.
- (11) Pelosi, C.; Agresti, G.; Santamaria, U.; Mattei, E. Artificial Yellow Pigments: Production and Characterization Through Spectroscopic Methods of Analysis. *e-Preservation Science* **2010**, *7*, 108–115.
- (12) Wanklyn, B. M.; Wondre, F. R.; Davison, W. Flux Growth of Crystals of Some Complex Oxides. *J. Mater. Sci. Lett.* **1984**, *3*, 539–543
- (13) Tite, M.; Pradell, T.; Shortland, A. Discovery, Production and Use of Tin-based Opacifiers in Glasses, Enamels and Glazes from the Late Iron Age Onwards: A Reassessment. *Archaeometry* **2008**, *50*, 67–84.
- (14) Clark, R. J. H.; Cridland, L.; Kariuki, B. M.; Harris, K. D. M.; Withnall, R. Synthesis, Structural Characterisation and Raman Spectroscopy of the Inorganic Pigments Lead Tin Yellow Types I and II and Lead Antimonate Yellow: their Identification on Medieval Paintings and Manuscripts. *J. Chem. Soc. Dalton* **1995**, 2577–2582.
- (15) Hashemi, T.; Brinkman, A. W.; Wilson, M. J. Preparation, Sintering and Electrical Behavior of Di-lead Stannate. *J. Mater. Sci. Lett.* **1992**, *11*, 666–668.
- (16) Catalano, J.; Yao, Y.; Murphy, A.; Zumbulyadis, N.; Centeno, S. A.; Dybowski, C. Nuclear Magnetic Resonance Spectra and ²⁰⁷Pb Chemical Shift Tensors of Lead Carboxylates Relevant to Soap Formation in Oil Paintings. *Appl. Spectrosc.* **2014**, *68*, 280–286.
- (17) MacGregor, A. W.; O'Dell, L. A.; Schurko, R. W. New Methods for the Acquisition of Ultra-Wideline Solid-State NMR Spectra of Spin-1/2 Nuclides. *J. Magn. Reson.* **2011**, 208, 103–13.
- (18) O'Dell, L. A.; Rossini, A. J.; Schurko, R. W. Acquisition of Ultrawideline NMR Spectra from Quadrupolar Nuclei by Frequency Stepped WURST-QCPMG. *Chem. Phys. Lett.* **2009**, *468*, 330–335.
- (19) O'Dell, L. A.; Schurko, R. W. QCPMG Using Adiabatic Pulses for Faster Acquisition of Ultra-wideline NMR Spectra. *Chem. Phys. Lett.* **2008**, 464, 97–102.
- (20) O'Dell, L. A. The WURST Kind of Pulses in Solid-state NMR. Solid State Nucl. Magn. 2013, 55-56, 28-41.
- (21) Tang, J. A.; O'Dell, L. A.; Aguiar, P. M.; Lucier, B. E. G.; Sakellariou, D.; Schurko, R. W. Application of Static Microcoils and WURST Pulses for Solid-state Ultra-wideline NMR Spectroscopy of Quadrupolar Nuclei. *Chem. Phys. Lett.* **2008**, 466, 227–234.
- (22) Pyykko, P. Relativistic Effects in Structural Chemistry. Chem. Rev. 1988, 88, 563-594.
- (23) Autschbach, J. Perspective: Relativistic effects. J. Chem. Phys. 2012, 136, 15.
- (24) Autschbach, J. The Calculation of NMR Parameters in Transition Metal Complexes. Struct. Bonding (Berlin) 2004, 112, 1–48.
- (25) Orendt, A. M.; Facelli, J. C. Solid-state Effects on NMR Chemical Shifts. In *Annu. Rep. NMR Spectrosc.*; Elsevier Academic Press Inc: San Diego, 2007; Vol. 62, pp 115–178.
- (26) Weber, J.; Gunne, J. Calculation of NMR Parameters in Ionic Solids by an Improved Self-consistent Embedded Cluster Method. *Phys. Chem. Chem. Phys.* **2010**, *12*, 583–603.
- (27) Bonhomme, C.; Gervais, C.; Babonneau, F.; Coelho, C.; Pourpoint, F.; Azais, T.; Ashbrook, S. E.; Griffin, J. M.; Yates, J. R.; Mauri, F.; et al. First-Principles Calculation of NMR Parameters Using the Gauge Including Projector Augmented Wave Method: A Chemist's Point of View. *Chem. Rev.* **2012**, *112*, 5733–5779.

- (28) Gavarri, J. R.; Vigouroux, J. P.; Calvarin, G.; Hewat, A. W. Structure of SnPb2O4 at 4 Temperatures the Relation between Thermal-Expansion and Thermal Agitation. *J. Solid State Chem.* **1981**, 36, 81–90.
- (29) Neue, G.; Dybowski, C.; Smith, M. L.; Hepp, M. A.; Perry, D. L. Determination of Pb-207(2+) chemical shift tensors from precise powder lineshape analysis. *Solid State Nucl. Magn. Reson.* **1996**, *6*, 241–250.
- (30) Kennedy, J. D.; McFarlane, W. In *Multinuclear NMR*; Mason, J., Ed.; Plenum Press: New York, 1987; pp 305–333.
- (31) Gabuda, S. P.; Kozlova, S. G.; Terskikh, V. V.; Dybowski, C.; Neue, G.; Perry, D. L. Pb-207 NMR of Minium, Pb3O4: Evidence for the Pb-2 (4+) Ion and Possible Relativistic Effects in the Pb-Pb Bond. *Solid State Nucl. Magn. Reson.* **1999**, *15*, 103–107.
- (32) Eichele, K. HBA 3.1 and WSOLIDS; University of Tubingen: Tubingen, 2013.
- (33) Haeberlen, U. High Resolution NMR in Solids; Academic Press: New York, 1976.
- (34) Mason, J. Conventions for the Reporting of Nuclear Magnetic Shielding (or Shift) Tensors Suggested by Participants in the NATO ARW on NMR Shielding Constants at the University-of-Maryland, College-Park, July 1992. *Solid State Nucl. Magn. Reson.* **1993**, *2*, 285–288.
- (35) ADF2013 SCM, Theoretical Chemistry; Vrije Universiteit: Amsterdam, The Netherlands, http://www.scm.com.
- (36) Guerra, C. F.; Snijders, J. G.; te Velde, G.; Baerends, E. J. Towards an Order-N DFT Method. *Theor. Chem. Acc.* **1998**, 99, 391–403.
- (37) te Velde, G.; Bickelhaupt, F. M.; Baerends, E. J.; Guerra, C. F.; Van Gisbergen, S. J. A.; Snijders, J. G.; Ziegler, T. Chemistry with ADF. *J. Comput. Chem.* **2001**, 22, 931–967.
- (38) Perdew, J. P. Density-Functional Approximation for the Correlation-Energy of the Inhomogeneous Electron-Gas. *Phys. Rev.* B 1986, 33, 8822–8824.
- (39) Becke, A. D. Density-Functional Exchange-Energy Approximation with Correct Asymptotic-Behavior. *Phys. Rev. A* **1988**, 38, 3098–3100.
- (40) van Lenthe, E.; Baerends, E. J.; Snijders, J. G. Relativistic Regular 2-Component Hamiltonians. *J. Chem. Phys.* **1993**, *99*, 4597–4610.
- (41) Lenthe, E. v.; Snijders, J. G.; Baerends, E. J. The zero-order regular approximation for relativistic effects: The effect of spin-orbit coupling in closed shell molecules. *J. Chem. Phys.* **1996**, *105*, 6505–6516
- (42) van Lenthe, E.; van Leeuwen, R.; Baerends, E. J.; Snijders, J. G. Relativistic Regular Two-component Hamiltonians. *Int. J. Quantum Chem.* **1996**, *57*, 281–293.
- (43) Wolff, S. K.; Ziegler, T.; van Lenthe, E.; Baerends, E. J. Density functional calculations of nuclear magnetic shieldings using the zeroth-order regular approximation (ZORA) for relativistic effects: ZORA nuclear magnetic resonance. *J. Chem. Phys.* **1999**, *110*, 7689–7698.
- (44) Ditchfield, R. Self-Consistent Perturbation-Theory of Diamagnetism 1. Gauge-Invariant Lcao Method for NMR Chemical Shifts. *Mol. Phys.* **1974**, *27*, 789–807.
- (45) Schreckenbach, G.; Ziegler, T. Calculation of NMR Shielding Tensors Using Gauge-Including Atomic Orbitals and Modern Density-Functional Theory. *J. Phys. Chem.* **1995**, *99*, 606–611.
- (46) Schreckenbach, G.; Ziegler, T. The Calculation of NMR Shielding Tensors Based on Density Functional Theory and the Frozen-core Approximation. *Int. J. Quantum Chem.* **1996**, *60*, 753–766.
- (47) Shimoni-Livny, L.; Glusker, J. P.; Bock, C. W. Lone Pair Functionality in Divalent Lead Compounds. *Inorg. Chem.* **1998**, *37*, 1853–1867.
- (48) Leciejewicz, J. On Crystal Structure of Tetragonal (Red) Pbo. Acta Crystallogr. 1961, 14, 1304.
- (49) Fayon, F.; Farnan, I.; Bessada, C.; Coutures, J.; Massiot, D.; Coutures, J. P. Empirical Correlations Between Pb-207 NMR

- Chemical Shifts and Structure in Solids. J. Am. Chem. Soc. 1997, 119, 6837-6843.
- (50) Alkan, F.; Dybowski, C. Calculation of Chemical-Shift Tensors of Heavy Nuclei: A DFT/ZORA Investigation of 199Hg Chemical-Shift Tensors in Solids, and the Effects of Cluster Size and Electronic-State Approximations. *Phys. Chem. Chem. Phys.* **2014**, *16*, 14298–14308.
- (51) Sebald, A.; Merwin, L. H.; Dollase, W. A.; Seifert, F. A Multinuclear, High-resolution Solid-state NMR-study of Sorensenite (Na4SnBe2(Si3O9.2H2O) and Comparsion with Wollastonite and Pectolite. *Phys. Chem. Miner.* **1990**, *17*, 9–16.
- (52) Clayden, N. J.; Dobson, C. M.; Fern, A. High-Resolution Solid-State Sn-119 Nuclear Magnetic-Resnonance Spectroscopy of Ternary Tin Oxides. *J. Chem. Soc. Dalton* **1989**, 843–847.
- (53) Cossement, C.; Darville, J.; Gilles, J. M.; Nagy, J. B.; Fernandez, C.; Amoureux, J. P. Chemical-shift Anisotropy and Indirect Coupling in SnO2 and SnO. *Magn. Reson. Chem.* **1992**, *30*, 263–270.
- (54) Kulshreshtha, S. K.; Sasikala, R.; Sudarsan, V. Non-random Distribution of Cations in Sn1-xTixO2 ($0.0 \le x \le 1.0$): a Sn-119 MAS NMR Study. *I. Mater. Chem.* **2001**, *11*, 930–935.
- (55) Robinet, L.; Corbeil, M. C. The Characterization of Metal Soaps. *Stud. Conserv.* **2003**, *48*, 23–40.